CORE
Metadata, citation and similar papers at core.ac.uk
Provided by Kyoto University Research Information Repository
KURENAI
Kyoto University Research Information Repository
KYOTO UNIVERSITY

Title	Light-Induced Degradation Mechanism in Poly(3-hexylthiophene)/Fullerene Blend Solar Cells
Author(s)	Tamai, Yasunari; Ohkita, Hideo; Namatame, Miki; Marumoto, Kazuhiro; Shimomura, Satoru; Yamanari, Toshihiro; Ito, Shinzaburo
Citation	Advanced Energy Materials (2016), 6(11)
Issue Date	2016-06-08
URL	http://hdl.handle.net/2433/217963
Right	This is the accepted version of the following article: [Tamai Y., Ohkita H., Namatame M., Marumoto K., Shimomura S., Yamanari T., Ito S. (2016). Light-Induced Degradation Mechanism in Poly(3-hexylthiophene)/Fullerene Blend Solar Cells. Advanced Energy Materials, 6, 11, 1600171], which has been published in final form at http://doi.org/10.1002/aenm.201600171. This article may be used for non-commercial purposes in accordance with Wiley Terms and Conditions for Self-Archiving.; The full-text file will be made open to the public on 8 June 2017 in accordance with publisher's 'Terms and Conditions for Self-Archiving'.; This is not the published version. Please cite only the published version. この論文は出版社版でありません。引用の際には出版社版をご確認ご利用ください。
Type	Journal Article
Textversion	author

Kyoto University

DOI: 10.1002/ ((please add manuscript number))
Article type: Full Paper

Light-Induced Degradation Mechanism in Poly(3-hexylthiophene)/Fullerene Blend Solar Cells

Yasunari Tamai, Hideo Ohkita, Miki Namatame, Kazuhiro Marumoto, Satoru Shimomura, Toshihiro Yamanari, Shinzaburo Ito*

Dr. Y. Tamai,[+] Dr. H. Ohkita, Prof. S. Ito
Department of Polymer Chemistry, Graduate School of Engineering, Kyoto University, Katsura, Nishikyo, Kyoto 615-8510, Japan
E-mail: ohkita@photo.polym.kyoto-u.ac.jp
M. Namatame, Prof. K. Marumoto
Division of Materials Science, University of Tsukuba, Tsukuba, Ibaraki 305-8573, Japan
Dr. S. Shimomura, Dr. T. Yamanari
Chemical Materials Evaluation and Research Base (CEREBA), Tsukuba, Ibaraki 305-8565, Japan
Dr. S. Shimomura
Advanced Materials Research Laboratories, Toray Industries, Inc., 3-2-1 Sonoyama, Otsu, Shiga 520-0842, Japan

[+] Present address: Cavendish Laboratory, University of Cambridge, J J Thomson Avenue, Cambridge CB3 0HE, United Kingdom

Keywords: Organic photovoltaics, Stability, Burn-in, Transient absorption, Electron spin resonance

Abstract: The mechanism of light-induced degradation in organic solar cells based on regioregular poly(3-hexylthiophene) and indene-C_{60} bisadduct is studied by transient absorption (TA) and electron spin resonance (ESR) measurements. After 45-hour light exposure under simulated solar illumination at 100 mW cm^{-2}, the short-circuit current density, open-circuit voltage, and fill factor are all degraded by about 20–30% relative to the initial photovoltaic parameters. For the assignment of limiting conversion processes in the degraded solar cells, exciton diffusion into a donor/acceptor interface, charge transfer at the interface, charge dissociation into free charge carriers, and charge collection to each electrode are observed before and after the light exposure by the TA measurement. As a result, it is found that the charge collection deteriorates after the light exposure because of light-induced charge

trap formation in the bulk of the active layer. The origin of charge traps is further discussed on the basis of ESR measurements and density functional theory calculation.

1. Introduction

Improving device stability has recently become the most important issue for practical use of organic solar cells while improving device efficiency has successfully led to a power conversion efficiency (PCE) over 10% even for single junction cells.[1–3] Several degradation mechanisms have been proposed such as reactions with oxygen or water.[4–6] Among them, light-induced photodegradation would be the most crucial issue to be solved because solar cells are inevitably operated under the light exposure. Recent studies have shown severe deterioration of photovoltaic efficiency down to 60% during the first 100-hour light exposure.[7] This is called burn-in photodegradation, which comprises a major obstacle to commercial use of organic solar cells. Thus, it is highly required to understand the burn-in loss mechanism. Recently, several mechanisms have been discussed for the burn-in photodegradation: photoinduced oxidation by oxygen atoms trapped in the films,[8–10] organic or inorganic impurities in the polymers (such as palladium catalysts, tin- or halogen-containing molecules, and unreacted monomers),[11–13] crosslinking or dimerization of materials,[14] and polaron trapping either at the interface between the active layer and electrode or in the bulk of the active layer.[15–19] In other words, the burn-in photodegradation mechanism is still open question.

For device stability tests, regioregular poly(3-hexylthiophene) (P3HT) and a soluble fullerene derivative, [6,6]-phenyl-C_{61}-butyric acid methyl (PCBM), have been used as benchmark materials. After thermal annealing, P3HT/PCBM solar cells have been reported to form large PCBM clusters in the active layer, resulting in less stable operation.[20,21] In contrast, polymer solar cells based on P3HT and indene-C_{60} bisadduct (ICBA) have been reported to be more stable even after thermal annealing.[22,23] This is probably because ICBA is unlikely

to form aggregates owing to two bulky indene side attachments. Thus, ICBA could be a better candidate for an alternate acceptor material to PCBM in terms of the thermal stability. On the other hand, photostability tests have also been performed using PCBM or [6,6]-phenyl-C_{71}-butyric acid methyl ester ($PC_{71}BM$). Although the burn-in photodegradation is observed for P3HT/PCBM and P3HT/$PC_{71}BM$ solar cells, no photostability studies have been reported for P3HT/ICBA solar cells. As is the case of thermal stability, the photostability may be improved by using ICBA instead of PCBM. If not, the photodegradation would originate from polymers rather than fullerenes. Further study is needed to settle this issue. Herein, we study burn-in photodegradation mechanisms in P3HT/ICBA solar cells. All the photovoltaic parameters, the short-circuit current density (J_{SC}), open-circuit voltage (V_{OC}), and fill factor (FF) decreased after the light exposure. In order to address the origin of J_{SC} and FF losses, we compare exciton diffusion into the donor/acceptor interface, charge transfer at the interface, charge dissociation into free charge carriers, and charge collection to each electrode before and after the photodegradation. We further discuss the mechanism of V_{OC} loss in terms of trap formation after the light exposure.

2. Experimental

2.1. Materials

Two kinds of P3HT were purchased from Rieke Metals, Inc. (4002-E) and from Plextronics (Plexcore OS 2100). The bromine contents in the P3HT were evaluated by X-ray fluorescence spectroscopy (see the Supporting Information). Here, we will denote P3HT from Rieke Metals as P3HT or standard P3HT, and P3HT from Plextronics as bromine-rich P3HT. ICBA and PCBM were purchased from Luminescence Technology Corp. and Solenne BV, respectively. All materials were used without further purification.

2.2. Device Fabrication

ITO-coated glass substrates with a size of 42 mm × 42 mm were cleaned by O_2 plasma treatment for 5 min. Poly(3,4-ethylenedioxythiophene):poly(4-styrenesulfonate) (PEDOT:PSS, Clevios PVP. AL 4083, Heareus Deutschland GmbH & Co. KG) was spin-coated (~20 nm) onto the substrates and dried on a hot plate under ambient air. Then, an active layer of P3HT/ICBA (1:0.7 by weight ratio) was spin-coated from chlorobenzene solution on the PEDOT:PSS coated ITO substrates in an N_2-filled glove box. The active layer thickness was 200 nm unless otherwise stated. Finally, an Al electrode of around 200 nm thickness and 49 mm^2 active area was deposited by vacuum evaporation at a rate of 1.5 nm s^{-1}. After the Al deposition, the device was thermally annealed on a digitally controlled hot plate in the glove box at 110 °C for 10 min, then cooled down to room temperature, and again thermally annealed at 140 °C for 30 min. All the devices were encapsulated in the glove box. For ESR measurements, rectangular ITO substrates with a size of 3 mm × 20 mm were used to insert the device into a sample tube with an inner diameter of 3.5 mm.[17] The active area of the cell was 2 mm × 10 mm. For the photodegradation test, the devices were exposed to AM1.5G simulated solar illumination under the open-circuit condition. Because device temperature was not controlled during the light exposure, the temperature might be higher than room temperature. However, the temperature rise did not affect phase-separated morphology at all as will be shown later, suggesting no impact on the device performance. Hereafter, we will denote the P3HT/ICBA blend cells before photodegradation as “fresh cell” and that after 45-hour light exposure as “degraded cell”.

2.3. Measurements

The current density–voltage (*J*–*V*) characteristics were measured with a source meter (Keithley, 2611B) in the dark and under AM1.5G simulated solar illumination at 100 mW cm^{-2}. The light intensity was calibrated using a standard cell for amorphous Si solar cells (Bunkokeiki, BS-520). The *J*–*V* characteristics were monitored every one hour during the

light exposure. Temperature dependence of the *J–V* characteristics was measured with a DC voltage and current source/monitor (Advantest, R6243) in a vacuum prober system (ALS Technology, VPS3-50) under the illumination from a 100 W Xe lamp (Asahi Spectra, LAX-C100) equipped with a uniform illumination lens unit (Asahi Spectra, RLQL80-0.5). Electroluminescence (EL) spectra from a photovoltaic cell were measured at room temperature with a fluorescence spectrophotometer (Horiba Jobin Yvon, NanoLog) equipped with a liquid-nitrogen-cooled InGaAs near-IR array detector (Horiba Jobin Yvon, Symphony II).

Femtosecond transient absorption (TA) data were collected with a pump and probe femtosecond transient spectroscopy system. This system consists of a transient absorption spectrometer (Ultrafast Systems, Helios), a regeneratively amplified Ti:sapphire laser (Spectra-Physics, Hurricane), and an ultrafast optical parametric amplifier (Spectra-Physics, TOPAS). The excitation pulse was set at 600 nm with a spot size of ~7 mm^2. Microsecond TA data were collected with a highly sensitive microsecond transient spectroscopy system. A dye laser (Photon Technology International Inc., GL-301) pumped by a nitrogen laser (Photon Technology International Inc., GL-3300) was used as an excitation source, which provides sub-nanoseconds pulses with various fluences from ~μJ to 0.1 mJ cm^{-2} at a repetition rate of 4 Hz. The excitation wavelength was set at 610 nm with a spot size of ~1 cm^2. TA measurements were carried out with transmission mode without metal electrode. Note that the TA spectra and dynamics were highly reproducible even after the several times measurements. In other words, the laser irradiation had negligible effects on the sample photodegradation at least under this experimental condition. Details of TA systems we employed are described elsewhere.[24–26]

Electron spin resonance (ESR) measurements were performed using an X-band spectrometer (JEOL-RESONANCE, JES-FA200) at 290 K. The number of spins, *g* factor, and linewidth of the ESR signal were calibrated using a standard Mn^{2+} marker sample. The absolute value

of the number of spins was calculated using a solution (220 μL) of 4-hydroxy-2,2,6,6-tetramethylpiperidin-1-oxyl (TEMPOL) as a standard. The calibration of the *g* factor was performed by using a software program of the ESR system considering high second order correction to the effective resonance field. Its correctness was also confirmed by using 2,2-diphenyl-1-picrylhydrazyl (DPPH) as another standard sample.[17]

3. Results and Discussion

3.1. Photovoltaic Properties

Figure 1 shows typical current density–voltage (*J*–*V*) characteristics of fresh (black) and degraded (red) P3HT/ICBA cells. The photovoltaic parameters are summarized in **Table 1**. Time evolutions of the photovoltaic parameters during the 45-hour light exposure are shown in **Figure S1**. As shown in Figure 1 and Table 1, J_{SC}, V_{OC}, and FF decreased to 79, 78, and 70%, respectively, after the light exposure. These decreases resulted in an approximately 60% reduction in the power conversion efficiency (PCE). On the other hand, no difference was found for a saturation current density J_{sat} at a reverse bias of −5 V before and after the degradation, suggesting that the loss in J_{SC} is ascribed to depressed charge dissociation and/or charge collection efficiency rather than charge photogeneration efficiency. We note that the photovoltaic characteristics were recovered to the initial values after baking the degraded cell at 130 °C for 20 min as shown in **Figure S2**. This is consistent with the previous report,[7] suggesting that the photodegradation does not originate from any irreversible damages of the device such as conjugation breaks or photoinduced oxidation of materials. We therefore hypothesize that the origin of the photodegradation is formation of charge traps as reported previously. For comparison, we performed the same degradation/recovery tests for P3HT/PCBM cell as shown in **Figure S3**. As a result, we found that there are no apparent difference about the photodegradation behavior between ICBA and PCBM. This finding

suggests that the burn-in photodegradation would be due to polymer materials rather than fullerenes.

3.2. Charge Generation Dynamics

First, we measured femtosecond TA to discuss how the charge generation dynamics impact on the loss in J_{SC}. **Figure 2** shows the TA spectra of fresh (panel a) and degraded (panel b) cells. As shown in the figure, the singlet exciton band was primarily observed at around 1200 nm as reported previously,[24,27] and then decayed in tens of picoseconds. Instead, polaron bands were observed at around 700 and 1000 nm, indicating exciton diffusion in P3HT crystalline domains followed by efficient charge transfer to ICBA. The absorption bands at 700 and 1000 nm are assigned to delocalized polarons generated in P3HT crystalline domains and localized polarons generated in P3HT disordered domains, respectively.[28,29] These polaron bands negligibly decayed on nanosecond time stage. **Figure 3** shows the time evolution of singlet excitons at 1400 nm, delocalized polarons at 700 nm, and localized polarons. Note that the time evolution of localized polarons was extracted by subtracting the transient signal at 1400 nm from that at 1000 nm after the signal at 0 ps is normalized because of negligible charge transfer at 0 ps upon crystalline selective excitation at 600 nm as discussed in ref 28. As shown in the figure, no difference in the charge generation dynamics was observed at all between the fresh and degraded cells, indicating that the loss in J_{SC} is not correlated to exciton diffusion, charge transfer, or charge dissociation. This finding is consistent with the comparable J_{sat} as mentioned above and is also indicative of no morphological change after the light exposure.

3.3. Charge Recombination Dynamics

We further measured TA measurements on microsecond time domains to discuss how the charge transport dynamics impact on the loss in J_{SC}. In this time domain, two polaron bands

were still observed at around 700 and 1000 nm (**Figure S4**). For the polaron band at 700 nm, as shown in **Figure 4a**, no difference in the decay dynamics was observed before and after the light exposure. For the polaron band at 1000 nm, as shown in Figure 4b, slower decay dynamics was additionally observed for the degraded cell at a longer time stage (>50 μs). These decay dynamics are well fitted with a power-law equation.

$$n(t) = \frac{n_0}{(1+at)^{\alpha}} \quad (1)$$

Here, the transient signal ΔOD is converted into the number density $n(t)$ on the basis of the Beer–Lambert law: $n(t) = \Delta OD(t)\, N_A (1000\varepsilon l)^{-1}$ where N_A is the Avogadro's constant, ε is the molar absorption coefficient (3.5×10^4 M^{-1} cm^{-1} at 700 nm and 3.0×10^4 M^{-1} cm^{-1} at 1000 nm),[29] and l is the film thickness. This power-law equation has been theoretically derived for bimolecular recombination in energetically disordered materials.[30,31] For the delocalized polaron band at 700 nm, the slope α is unity ~1 before and after the light exposure, suggesting negligible charge trap formation in crystalline domains even after the light exposure. For the localized polaron band at 1000 nm, on the other hand, the slope α is unity ~1 before the light exposure and ~0.4 after the light exposure, suggesting charge trap formation in amorphous domains after the light exposure.[29] A similar slower decay dynamics has been reported for blend films based on bromine end-capped P3HT and PCBM.[32] We thus speculate that the photodegradation we observed would result from trapped charges due to residual bromines at P3HT chain ends as will discuss later. From the extrapolation of the slower decay to $t = 0$, we roughly estimate the trap density to be on the order of ~3×10^{16} cm^{-3}. The trap density was independent of the active layer thickness as shown in **Figure S5b**, suggesting that charge traps are not localized at the interface of the active layer and electrode but rather are uniformly formed in the bulk of the active layer. Transient photovoltage/photocurrent (TPV/TPC) measurements also indicate the charge trap formation after the light exposure. As shown in **Figure S6**, the charge extraction time was

longer in the degraded cell than in the fresh one. Interestingly, as shown by the green line in Figure 4b, the slower decay component disappeared after the degraded cell was baked at 130 °C for 20 min. In summary, these findings suggest that the losses in J_{SC} and FF would be caused by charge traps formed in P3HT disorder domains as will be discussed later.

3.4. Charge Transfer State Energy

We next focus on the V_{OC} loss observed in the degraded cell. We measured the EL spectra of the fresh and degraded cells to evaluate the charge transfer (CT) state energy. **Figure 5** shows the CT state emission of the fresh and degraded cells. In the framework of Marcus theory taking into account interfacial disorder, the spectral line shape of the CT emission is given by

$$\frac{I(E)}{E} = \frac{f}{\sqrt{2\pi\left(\sigma^2 + 2\lambda k_B T\right)}} \exp\left[-\frac{\left(E_{CT} - \lambda - E\right)^2}{2\left(\sigma^2 + 2\lambda k_B T\right)}\right] \quad (2)$$

where f is proportional to the square of the electronic coupling matrix element, k_B is Boltzmann constant, T is the absolute temperature, E_{CT} is the CT state energy, λ is reorganization energy associated with the CT state emission, and σ is energetic disorder of the CT state at the interface.[33–35] No difference in the EL spectra was observed for the fresh and degraded cells. The CT state energy is evaluated to be 1.39 eV with λ = 0.23 eV and σ = 0.06 eV for both cells. On the other hand, as shown in Figure 5b, the EL intensity drastically decreased under the same current density after the light exposure. These findings indicate that "dark" recombination sites are generated after the light exposure while the "emissive" CT state remains the same. Interestingly, the reduced EL intensity of the degraded cell was recovered to the original intensity observed for the fresh cell after the cell was baked at 130 °C for 20 min. This is again consistent with the recovery of the degraded device parameters and the disappearance of the slower decay of localized polarons on a microsecond time domain.

In order to evaluate the CT state energy of "dark" recombination sites, we measured the temperature dependence of the *J*–*V* characteristics as shown in **Figure 6**. Under the open-circuit condition, the applied voltage is equal to the difference between the quasi-Fermi levels of donor and acceptor materials. Thus, the temperature dependence of the V_{OC} is given by

$$qV_{OC} = E_g^{eff} - k_B T \ln\left(\frac{N_0^2}{n_e n_h}\right) \quad (3)$$

where E_g^{eff} is the effective bandgap of the blend system, which is a good measure for the E_{CT}, n_e and n_h are the electron and hole densities in the acceptor and donor, respectively, and N_0 is the density of electronic states in the cell.[34–37] Consequently, the E_g^{eff} can be evaluated by linear extrapolation to 0 K when the product $n_e n_h$ is constant independently of temperature. As reported previously, P3HT/PCBM solar cells meet these conditions because of temperature-independent charge generation above 100 K.[38,39] This would be true for our devices because the light exposure has no impact on the charge generation dynamics as mentioned above. For the fresh cell, as summarized in **Table 2**, the E_g^{eff} was evaluated to be 1.0 – 1.1 eV, which is consistent with previous reports,[40] although the data sets were limited to only 4 points because of faster degradation of our devices at lower temperatures. For the degraded cell, the E_g^{eff} was evaluated to be ~0.8 eV. This apparent decrease in the E_g^{eff} by ~0.2 – 0.3 eV is consistent with the decrease in the qV_{OC}, suggesting that the origin of the V_{OC} loss is the formation of charge traps with lower energy in P3HT disorder domains.

3.5. Origin of Charge Traps

We further performed light-induced ESR (LESR) measurements of the degraded cell in order to discuss the origin of charge traps. The LESR spectrum is obtained by subtracting the ESR spectrum of the fresh cell measured in the dark from that of the degraded cell under simulated solar illumination, which enables us to obtain ESR signals from only photogenerated species. In this measurement, a continuous-wave method with a modulation frequency of 100 kHz was

used for the external magnetic field. In other words, the signals observed here were due to photogenerated charge carriers with a lifetime of >10 μs. Here, the *g* factor was evaluated from the resonance magnetic field where the ESR spectrum with a first derivative form has a value of zero, and the peak-to-peak ESR linewidth ΔH_{pp} value was evaluated as the difference between the two magnetic fields at a peak and valley in the ESR spectrum. As shown by the black line in **Figure S8a**, the *g* factor and ΔH_{pp} in the ESR spectrum of the fresh cell were evaluated to be 2.00221 and 0.476 mT, respectively, which are consistent with those of P3HT hole polarons as reported previously.[17,41] **Figure 7a** shows the LESR spectrum of the standard P3HT/PCBM solar cells. As shown in the figure, a broad and weak signal was additionally emerged after the light exposure, suggesting formation of deeply trapped immobile charge species. As mentioned before, we speculate that the photodegradation we observed would result from trapped charges due to residual bromines at P3HT chain ends. We therefore measured LESR spectra of bromine-rich P3HT/ICBA blend cells in order to confirm our speculation. **Figure 7b** shows the LESR spectrum of the bromine-rich P3HT/ICBA blend cell. The broad signal became more apparently where the *g* factor and ΔH_{pp} of the broad signal were evaluated to be 2.00336 and 1.13 mT, respectively. These values are in good agreement with those obtained from DFT calculation for thiophene oligomers attached with or without bromine atoms (see the Supporting Information). As shown in **Tables S3** and **S4**, larger *g* factor and hyperfine coupling (hfc) constants are found for thiophene oligomers attached with bromine atoms.[42] In other words, these larger *g* factor and ΔH_{pp} observed for the degraded cell suggest that hole polarons are deeply trapped at around bromine residuals during the light exposure. We therefore conclude that the origin of light-induced trap formation is caused by residual bromine atoms at the chain ends that are likely to be located in disorder domains. Further experiments to reveal the formation mechanism of the bromine-induced traps are currently in progress, and will be reported in a separate paper.

4. Conclusion

We have discussed photodegradation mechanism of P3HT/ICBA blend cells on the basis of TA and ESR measurements. All the fundamental photovoltaic conversion processes were observed before and after the photodegradation by the TA measurements. As a result, we found that the light exposure has no impact on the charge generation including exciton diffusion into the P3HT/ICBA interface, charge transfer from P3HT to ICBA, and charge dissociation into free charge carriers. In addition, we found that the charge collection efficiency is decreased by charge trap formation in P3HT disorder domains after the photodegradation. On the basis of ESR measurement and DFT calculation, we assign the trap sites formed in disorder domains to bromine residuals at P3HT chain ends. We therefore conclude that the losses in J_{SC} and FF are due to the decrease in the charge collection efficiency because of trap formation at the P3HT chain ends, and that the loss of V_{OC} is ascribed to the formation of such deep recombination sites. We propose that the burn-in loss could be suppressed by increasing polymer molecular weight and/or crystallinity.

Supporting Information

Supporting Information is available from the Wiley Online Library or from the author.

Acknowledgments

This study is based on results obtained from a project commissioned by the New Energy and Industrial Technology Development Organization (NEDO).

Received: ((will be filled in by the editorial staff))
Revised: ((will be filled in by the editorial staff))
Published online: ((will be filled in by the editorial staff))

[1] S.-H. Liao, H.-J. Jhuo, P.-N. Yeh, Y.-S. Cheng, Y.-L. Li, Y.-H. Lee, S. Sharma, S.-A. Chen, *Sci. Rep.* **2014**, *4*, 6813.

[2] Y. Liu, J. Zhao, Z. Li, C. Mu, W. Ma, H. Hu, K. Jiang, H. Lin, H. Ade, H. Yan, *Nat. Commun.* **2014**, *5*, 5293.

[3] V. Vohra, K. Kawashima, T. Kakara, T. Koganezawa, I. Osaka, K. Takimiya, H. Murata, *Nat. Photon.* **2015**, *9*, 403.

[4] M. Jørgensen, K. Norrman, F. C. Krebs, *Sol. Energy Mater. Sol. Cells* **2008**, *92*, 686.

[5] M. Jørgensen, K. Norrman, S. A. Gevorgyan, T. Tromholt, B. Andreasen, F. C. Krebs, *Adv. Mater.* **2012**, *24*, 580.

[6] J. U. Lee, J. W. Jung, J. W. Jo, W. H. Jo, *J. Mater. Chem.* **2012**, *22*, 24265.

[7] T. Yamanari, H. Ogo, T. Taima, J. Sakai, J. Tsukamoto, Y. Yoshida, in Photovoltaic Specialists Conf. (PVSC), 2010 35th IEEE, IEEE, **2010**, 001628.

[8] J. Schafferhans, A. Baumann, A. Wagenpfahl, C. Deibel, V. Dyakonov, *Org. Electron.* **2010**, *11*, 1693.

[9] A. Seemann, T. Sauermann, C. Lungenschmied, O. Armbruster, S. Bauer, H.-J. Egelhaaf, J. Hauch, *Sol. Energy* **2011**, *85*, 1238.

[10] J. Razzell-Hollis, J. Wade, W. C. Tsoi, Y. Soon, J. Durrant, J.-S. Kim, *J. Mater. Chem. A* **2014**, *2*, 20189.

[11] W. R. Mateker, J. D. Douglas, C. Cabanetos, I. T. Sachs-Quintana, J. A. Bartelt, E. T. Hoke, A. E. Labban, P. M. Beaujuge, J. M. J. Fréchet, M. D. McGehee, *Energy Environ. Sci.* **2013**, *6*, 2529.

[12] J. Kong, S. Song, M. Yoo, G. Y. Lee, O. Kwon, J. K. Park, H. Back, G. Kim, S. H. Lee, H. Suh, K. Lee, *Nat. Commun.* **2014**, *5*, 5688.

[13] C. Bracher, H. Yi, N. W. Scarratt, R. Masters, A. J. Pearson, C. Rodenburg, A. Iraqi, D. G. Lidzey, *Org. Electron.* **2015**, *27*, 266.

[14] A. Distler, T. Sauermann, H.-J. Egelhaaf, S. Rodman, D. Waller, K.-S. Cheon, M. Lee, D. M. Guldi, *Adv. Energy Mater.* **2014**, *4*, 1300693.

[15] K. Kawano, C. Adachi, *Adv. Funct. Mater.* **2009**, *19*, 3934.

[16] C. H. Peters, I. T. Sachs-Quintana, W. R. Mateker, T. Heumueller, J. Rivnay, R. Noriega, Z. M. Beiley, E. T. Hoke, A. Salleo, M. D. McGehee, *Adv. Mater.* **2012**, *24*, 663.

[17] T. Nagamori, K. Marumoto, *Adv. Mater.* **2013**, *25*, 2362.

[18] T. Heumueller, W. R. Mateker, I. T. Sachs-Quintana, K. Vandewal, J. A. Bartelt, T. M. Burke, T. Ameri, C. J. Brabec, M. D. McGehee, *Energy Environ. Sci.* **2014**, *7*, 2974.

[19] T. Heumueller, T. M. Burke, W. R. Mateker, I. T. Sachs-Quintana, K. Vandewal, C. J. Brabec, M. D. McGehee, *Adv. Energy Matter.* **2015**, *5*, 1500111.

[20] J. Jo, S.-S. Kim, S.-I. Na, B.-K. Yu, D.-Y. Kim, *Adv. Funct. Mater.* **2009**, *19*, 866.

[21] W.-R. Wu, U.-S. Jeng, C.-J. Su, K.-H. Wei, M.-S. Su, M.-Y. Chiu, C.-Y. Chen, W.-B. Su, C.-H. Su, A.-C. Su, *ACS Nano* **2011**, *5*, 6233.

[22] Y.-H. Lin, Y.-T. Tsai, C.-C. Wu, C.-H. Tsai, C.-H. Chiang, *Org. Electron.* **2012**, *13*, 2333.

[23] P. Kumar, C. Bilen, K. Feron, X. Zhou, W. J. Belcher, P. C. Dastoor, *Appl. Phys. Lett.* **2014**, *104*, 193905.

[24] Y. Tamai, Y. Matsuura, H. Ohkita, H. Benten, S. Ito, *J. Phys. Chem. Lett.* **2014**, *5*, 399.

[25] Y. Tamai, K. Tsuda, H. Ohkita, H. Benten, S. Ito, *Phys. Chem. Chem. Phys.* **2014**, *16*, 20338.

[26] H. Ohkita, Y. Tamai, H. Benten, S. Ito, *IEEE J. Sel. Top. Quantum Electron.* **2016**, *22*, 4100112.

[27] J. Guo, H. Ohkita, H. Benten, S. Ito, *J. Am. Chem. Soc.* **2010**, *131*, 16869.

[28] J. Guo, H. Ohkita, H. Benten, S. Ito, *J. Am. Chem. Soc.* **2010**, *132*, 6154.

[29] J. Guo, H. Ohkita, S. Yokoya, H. Benten, S. Ito, *J. Am. Chem. Soc.* **2010**, *132*, 9631.

[30] J. Nelson, *Phys. Rev. B* **2003**, *67*, 155209.

[31] M. Tachiya, K. Seki, *Phys. Rev. B* **2010**, *82*, 085201.

[32] Y. Kim, S. Cook, J. Kirkpatrick, J. Nelson, J. R. Durrant, D. D. C. Bradley, M. Giles, M. Heeney, R. Hamilton, I. McCulloch, *J. Phys. Chem. C* **2007**, *111*, 8137.

[33] T. Burke, S. Sweetnam, K. Vandewal, M. McGehee, *Adv. Energy Mater.* **2015**, *5*, 1500123.

[34] K. Vandewal, K. Tvingstedt, A. Gadisa, O. Inganäs, J. V. Manca, *Phys. Rev. B* **2010**, *81*, 125204.

[35] K. Vandewal, K. Tvingstedt, A. Gadisa, O. Inganäs, J. Manca, *Phys. Rev. B* **2010**, *81*, 125204.

[36] S. R. Cowan, A. Roy, A. J. Heeger, *Phys. Rev. B* **2010**, *82*, 245207.

[37] K. Kawashima, Y. Tamai, H. Ohkita, I. Osaka, K. Takimiya, *Nat. Commun.* **2015**, *6*, 10085.

[38] F. Gao, W. Tress, J. Wang, O. Inganäs, *Phys. Rev. Lett.* **2015**, *114*, 128701.

[39] R. Mauer, I. A. Howard, F. Laquai, *J. Phys. Chem. Lett.* **2010**, *1*, 3500.

[40] J.-L. Wu, F.-C. Chen, M.-K. Chung, K.-S. Tan, *Energy Environ. Sci.* **2011**, *4*, 3374.

[41] S. Watanabe, H. Tanaka, S. Kuroda, A. Toda, S. Nagano, T. Seki, A. Kimoto, J. Abe, *Appl. Phys. Lett.* **2010**, *96*, 173302.

[42] D. Son, K. Marumoto, T. Kizuka, Y. Shimoi, *Synth. Met.* **2012**, *162*, 2451.

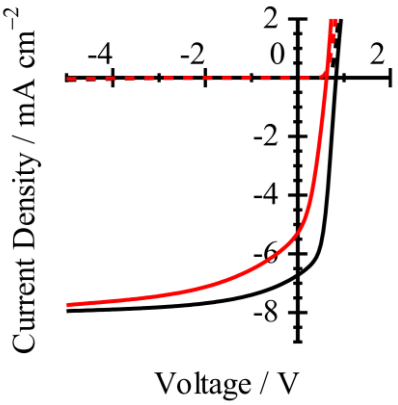

Figure 1. *J*–*V* characteristics of fresh (black) and degraded (red) P3HT/ICBA cells in the dark (broken lines) and under AM1.5G simulated solar illumination at 100 mW cm^{-2} (solid lines).

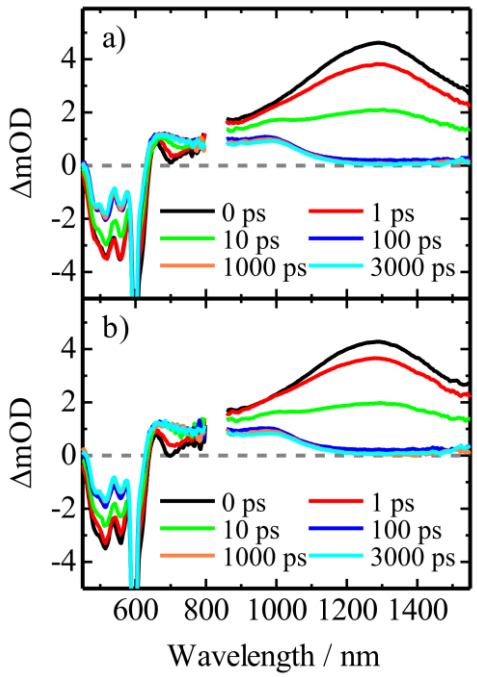

Figure 2. TA spectra of the a) fresh and b) degraded P3HT/ICBA blend cells. The excitation wavelength was set at 600 nm with a fluence of 2 μJ cm^{-2}.

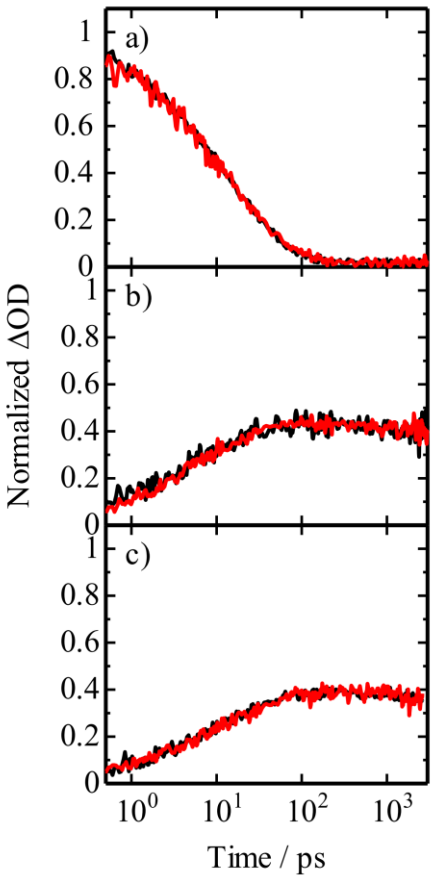

Figure 3. TA decays of the fresh (black) and degraded (red) P3HT/ICBA blend cells: a) singlet exciton at 1400 nm, b) delocalized polaron at 700 nm, and c) localized polaron. The time evolution of localized polaron was extracted by subtracting the transient signal at 1400 nm from that at 1000 nm after the signal at 0 ps is normalized.

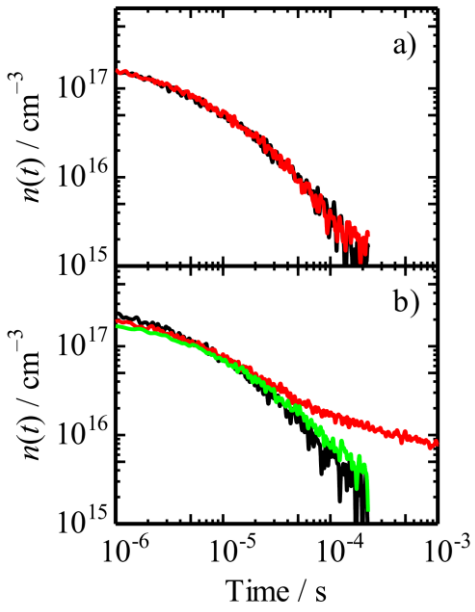

Figure 4. Charge recombination dynamics of the P3HT/ICBA blend cell with an active layer thickness of 100 nm: a) delocalized polaron at 700 nm, and b) localized polaron at 1000 nm. The black and red lines represent decay dynamics in the fresh (black) and degraded (red) cells. The green line in the panel b is polaron decay obtained after the degraded cell is baked at 130 °C for 20 min. The excitation wavelength was set at 610 nm with a fluence of 0.6 μJ cm^{-2}.

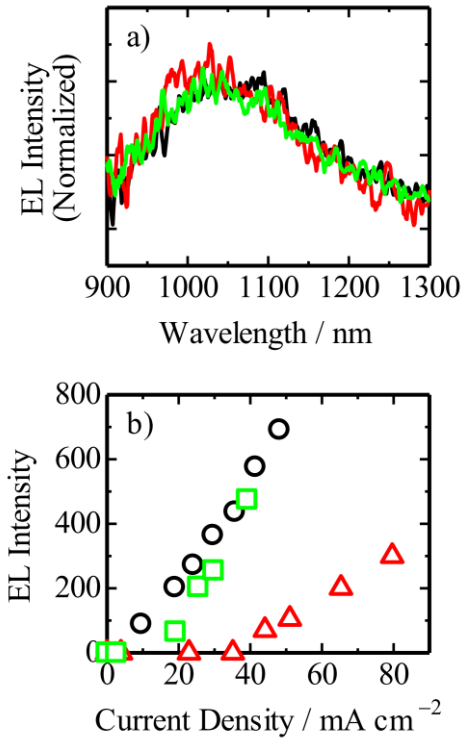

Figure 5. a) EL spectra of fresh (black), degraded (red), and baked (green) cells with an active layer thickness of 100 nm. b) EL peak counts against the current density. The legends of the symbols are the same as those in the panel a.

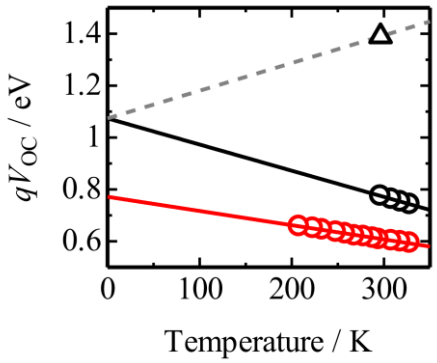

Figure 6. Temperature dependence of the V_{OC} for fresh (black circles) and degraded (red circles) cells. The solid lines represent the best fitting curves with the linear relationship (Equation 3). The triangle represents the emissive CT state energy evaluated from the EL spectrum.

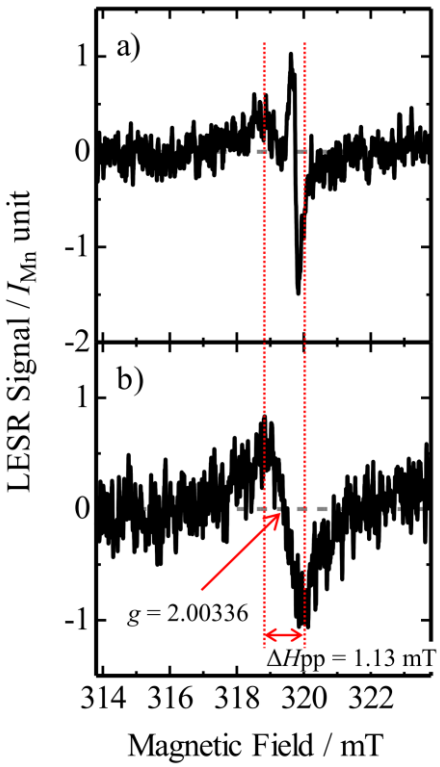

Figure 7. LESR signals of a) standard P3HT/ICBA and b) bromine-rich P3HT/ICBA cells after 5.5-h light exposure.

Table 1. Average device parameters for P3HT/ICBA blend cells before and after the photodegradation

Sample	J_{SC} [mA cm^{-2}]	V_{OC} [V]	FF	PCE [%]
Fresh	6.75	0.80	0.54	2.91
Degraded	5.30 (79%)	0.62 (78%)	0.38 (70%)	1.25 (43%)

[a] Values in parentheses in the bottom row represent retention of each photovoltaic parameter from their initial values.

Table 2. Summary of interfacial energy and their difference from V_{OC}

sample	E_{CT}[a] [eV]	E_g^{eff} [eV]	qV_{OC} [eV]	$E_{CT} - qV_{OC}$ [eV]	$E_g^{eff} - qV_{OC}$ [eV]
Fresh	1.39	1.0 – 1.1	0.78	0.61	0.2 – 0.3
Degraded	1.39	0.8	0.61	0.78	0.16

[a] "Emissive" CT state energy estimated from the EL spectra.

Photodegradation mechanism in regioregular poly(3-hexylthiophene)/indene-C_{60} bisadduct (P3HT/ICBA) blend cell is studied. After 45-hour solar cell operation under AM1.5G simulated solar illumination, photovoltaic efficiency drops by ~60%. The origin of the photodegradation is attributed to charge trap formation during the light exposure. Light-induced charge traps are generated in the P3HT disorder domains, most probably because of residual bromine atoms at P3HT chain ends.

Keyword: Organic photovoltaics, Stability, Burn-in, Transient absorption, Electron spin resonance

Y. Tamai, H. Ohkita*, M. Namatame, K. Marumoto, S. Shimomura, T. Yamanari, S. Ito

Light-Induced Degradation Mechanism in Poly(3-hexylthiophene)/Fullerene Blend Solar Cells

ToC figure ((Please choose one size: 55 mm broad × 50 mm high **or** 110 mm broad × 20 mm high. Please do not use any other dimensions))

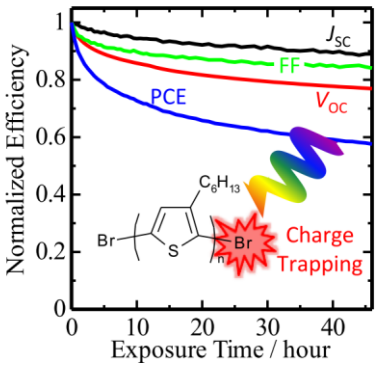

Copyright WILEY-VCH Verlag GmbH & Co. KGaA, 69469 Weinheim, Germany, 2013.

Supporting Information

Light-Induced Degradation Mechanism in Poly(3-hexylthiophene)/Fullerene Blend Solar Cells

Yasunari Tamai, Hideo Ohkita, Miki Namatame, Kazuhiro Marumoto, Satoru Shimomura, Toshihiro Yamanari, Shinzaburo Ito*

S1. X-ray fluorescence spectroscopy

To evaluate bromine content of P3HT, we carried out energy dispersive X-ray fluorescence spectroscopy. The same amount of P3HT powder from Rieke Metals and Plextronics was prepared in each sample holder. An X-ray fluorescence spectrometer (Hitachi High-Tech Science, EA1000VX) was used for this purpose. The measurement time was 600 s. The Br Kα intensities of each P3HT samples are summarized in **Table S1**.

Table S1. Bromine contents in P3HT.

sample	Intensity [cps]	Standard deviation
Standard P3HT (Rieke Metals)	836.7	1.2
Bromine-rich P3HT (Plextronics)	2436.2	1.8

S2. Time evolution of photovoltaic properties

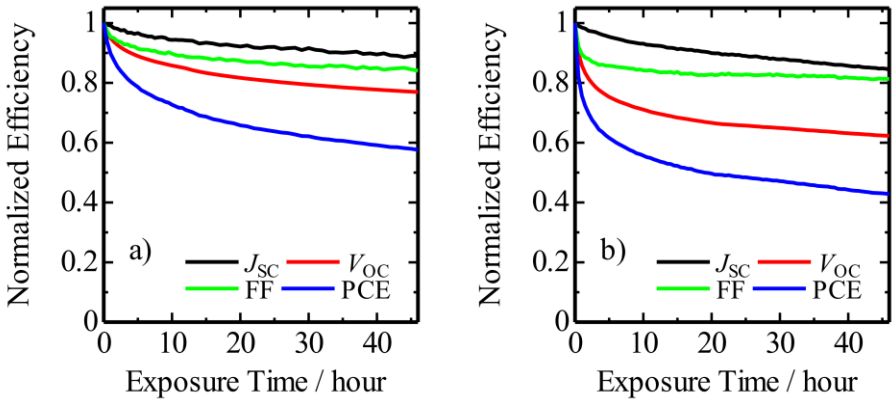

Figure S1. Normalized time evolution of a) P3HT/ICBA and b) P3HT/PCBM solar cells (100-nm-thick) under AM1.5G simulated solar illumination at 100 mW cm^{-2}: J_{SC} (black), V_{OC} (red), FF (green), and PCE (blue).

S3. Photovoltaic properties after baking

Figure S2 shows typical *J–V* characteristics of fresh (black) and degraded (red) P3HT/ICBA cells with an active layer thickness of 100 nm. The photovoltaic characteristics were recovered to the initial values after the degraded cell was baked at 130 °C for 20 min as shown by the green line. The same degradation/recovery behavior was observed for P3HT/PCBM cells as shown in **Figure S3**.

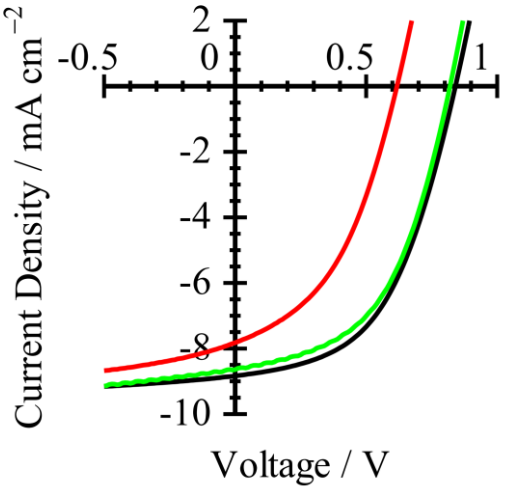

Figure S2. *J–V* characteristics of fresh (black) and degraded (red) P3HT/ICBA solar cells with an active layer thickness of 100 nm. The green line is the *J–V* characteristics after the degraded cell was baked at 130 °C for 20 min.

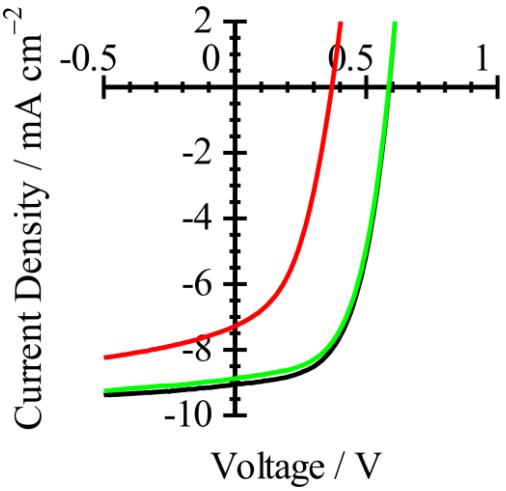

Figure S3. *J–V* characteristics of fresh (black) and degraded (red) P3HT/PCBM solar cells with an active layer thickness of 100 nm. The green line is the *J–V* characteristics after the degraded cell was baked at 130 °C for 20 min.

S4. Microsecond TA measurements

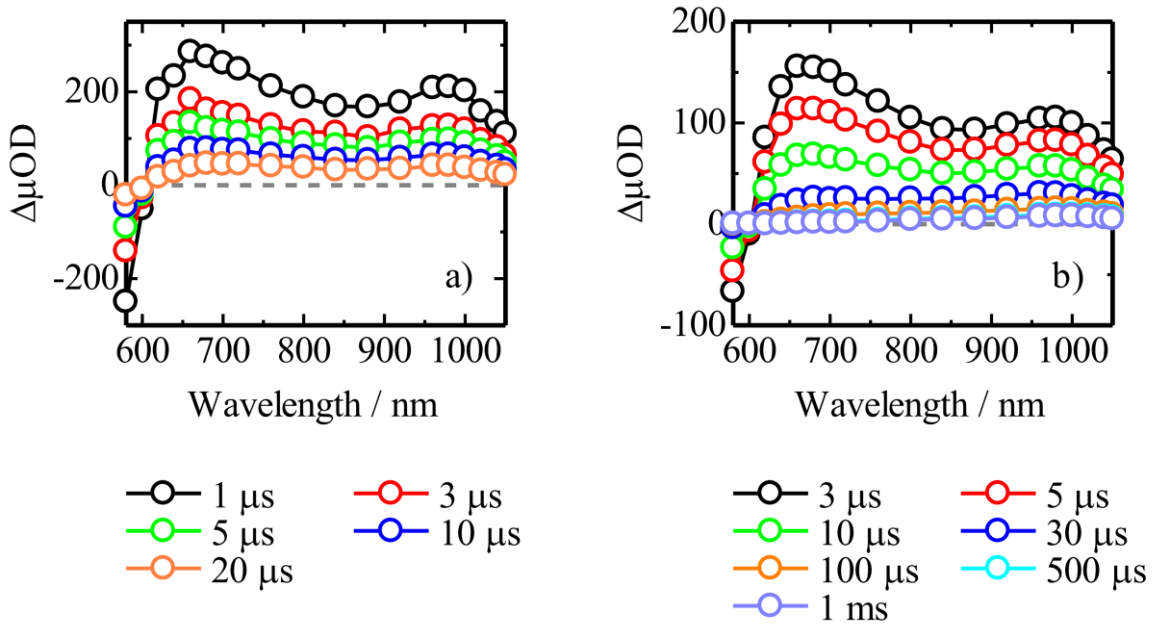

Figure S4. TA spectra of a) fresh and b) degraded P3HT/ICBA blend cells. The excitation wavelength was set at 610 nm with a fluence of 1.6 μJ cm^{-2}.

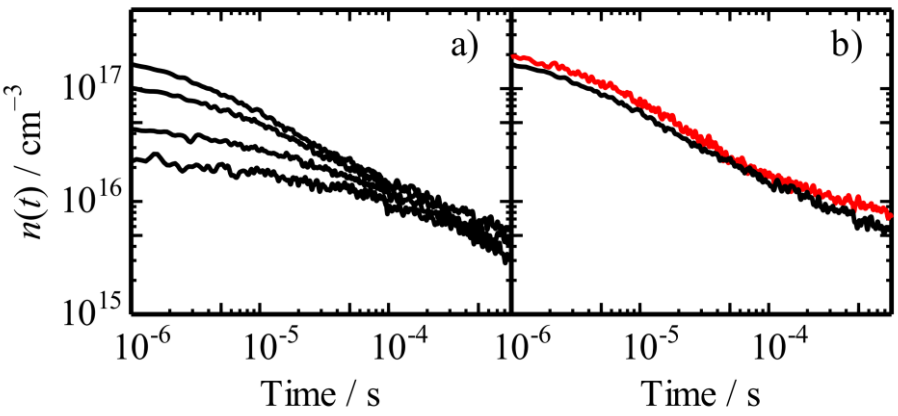

Figure S5. a) Transient decays of localized polarons in P3HT/ICBA degraded cells (200-nm-thick) excited with a fluence of 0.13 to 1.6 μJ cm^{-2} from bottom to top in the panel. b) Transient decays of localized polarons in P3HT/ICBA degraded cells with an active layer thickness of 200 nm (black) and 100 nm (red).

S5. Charge carrier lifetime and charge extraction time

Charge carrier lifetime under the open-circuit condition was measured by transient photovoltage/photocurrent (TPV/TPC) techniques. **Figure S6a** shows the charge carrier lifetime plotted against charge carrier density. The charge carrier lifetime under the 1 sun condition was estimated to be 4.7 μs for the fresh cell and 8.5 μs for the degraded cell. The lifetime of the fresh cell is much shorter than that reported for P3HT-based cell.[S1] This result suggests that morphology of our cell was not optimized partly becauese of the non-ideal blend ratio (1:0.7 by weight) and bisadduct (less crystalline) fullerene. The lifetime of the degraded cell is slightly longer than that of the fresh one, which is not remarkable but highly reproducible. This is probably because of the reduction in charge mobility after the degradation. Note that carrier density of the degraded cell under the 1 sun condition was slightly lower than that of the fresh cell. This is probably because of imcomplete charge collection under the TPC measurement, resulting in underestimate of the charge density.

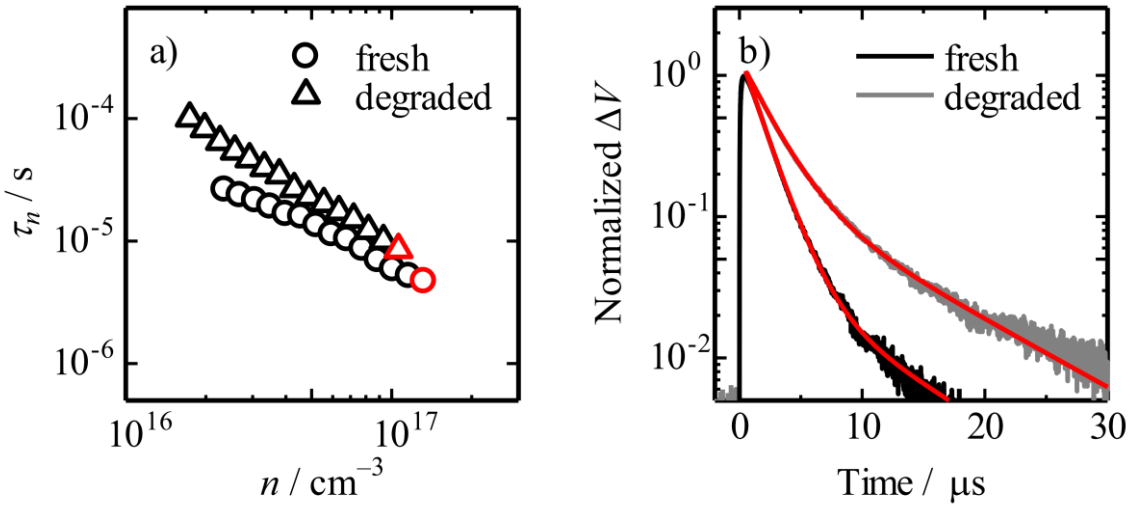

Figure S6. a) Charge carrier lifetime under the open-circuit condition plotted against carrier density. The red symbols represent the lifetime under 1 sun condition. b) Time evolution of laser induced voltage rise under the short-circuit condition.

Figure S6b shows the time evolution of transient photovoltage under the short-circuit condition. These decays were fitted with two exponential functions as shown by the red lines. The lifetimes (and their fractions) are summarised in **Table S2**. At the short-circuit condition, transient photovoltage decay is mainly attributed to the charge collection to electrodes. Thus, the faster components correspond to the charge extraction time. On the other hand, the slower components are comparable to the charge carrier lifetime under the open-circuit condition evaluated by the TPV measurements. We thus attribute to trapped charges, which are not

collected to the electrode but rather recombine to the ground state. The fraction of the slower component increased after the light exposure, which is consistent with the J_{SC} loss we observed.

Table S2. Charge carrier lifetimes (and their fractions) in fresh and degraded cells.

sample	τ_1 [μs]	τ_2 [μs]
fresh	1.6 (97%)	8.0 (3%)
degraded	2.3 (87%)	9.0 (13%)

S6. LESR measurements

Figure S7a shows typical *J–V* characteristics of standard (black) and bromine-rich (red) P3HT/ICBA cells fabricated on rectangular ITO substrates with a size of 3 mm × 20 mm. Time evolutions of the J_{SC} during the 6-hour light exposure are shown in **Figure S7b**. The device parameters fabricated on the rectangular ITO substrates are typically lower than that of normal cells (42 mm × 42 mm) primarily because of the difficulty in device fabrications as reported previously.[S2] Nonetheless, these devices exhibited similar degradation behavior as reported.

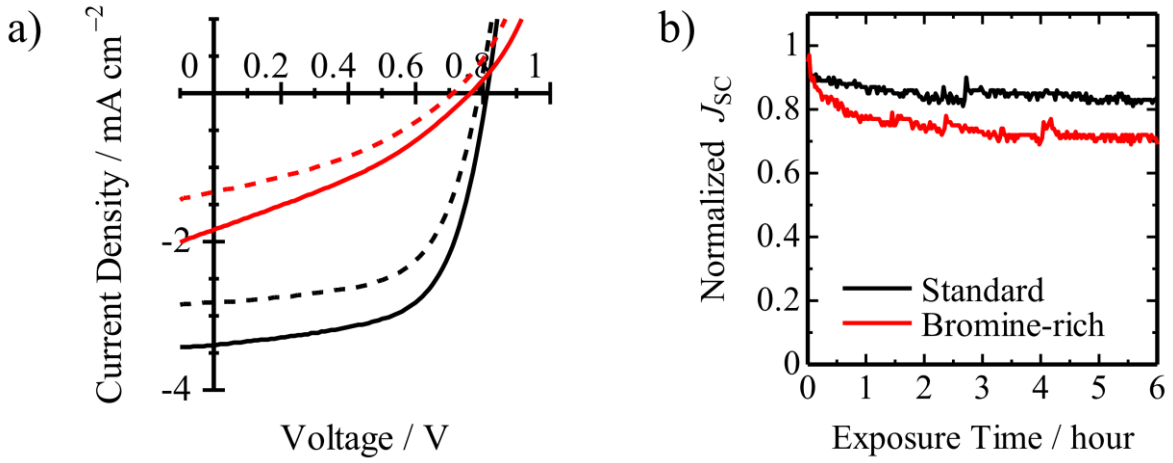

Figure S7. a) *J–V* characteristics of standard (black) and bromine-rich (red) P3HT/ICBA solar cells on rectangular ITO substrates with a size of 3 mm × 20 mm before (solid) and after (broken) simulated solar illumination, and b) Normalized time evolution of J_{SC} during the LESR measurements.

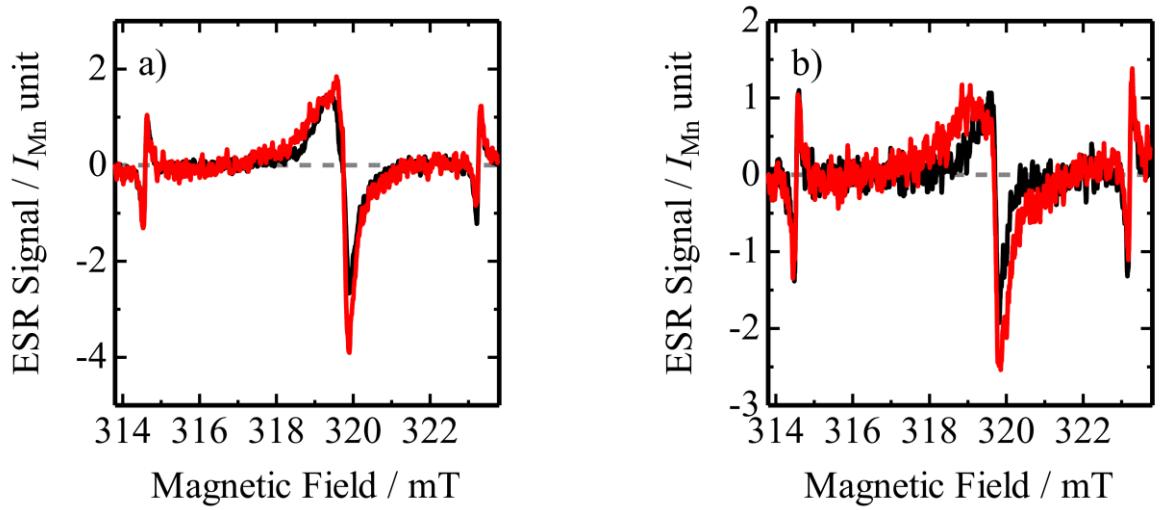

Figure S8. ESR signals of a) standard P3HT/ICBA and b) bromine-rich P3HT/ICBA cells. The black and red lines represent the ESR spectrum of the fresh cell in the dark and that of the degraded cell under simulated solar illumination, respectively.

S7. Density functional theory (DFT) calculation

DFT calculations were carried out for the hole polaron states of isolated thiophene hexamer (6T-H_2), bromine-monosubstituted 6T at one chain end (6T-HBr), and bromine-bissubstituted 6T at both chain ends (6T-Br_2) as shown in **Figure S9**. Those structures in the polaron states were optimized using UB3LYP functional and 6-31+G(d,p) basis set. The *g* tensors and hyperfine coupling (hfc) constants were calculated with the gauge-independent atomic orbitals (GIAO). All the calculation were performed using Gaussian 09, Revision D.01.[S3]

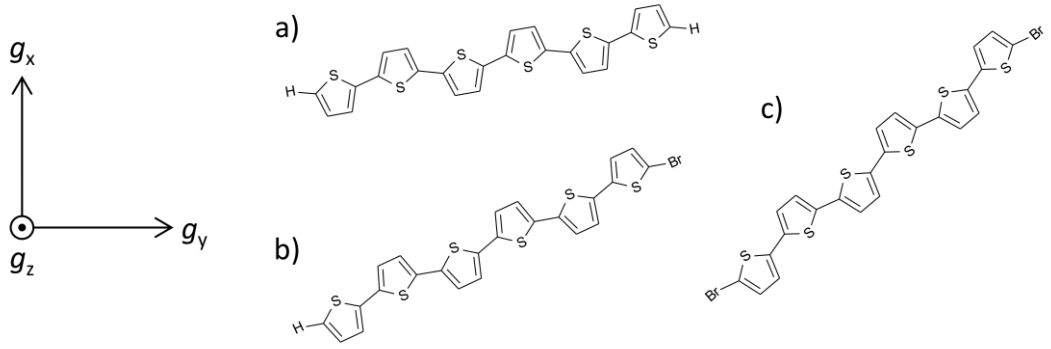

Figure S9. Chemical structures of a) 6T-H_2, b) 6T-HBr, and c) 6T-Br_2. Molecular principal axises were set as X: molecular short axis, Y: molecular long axis, Z: perpendicular to molecular plane.

Table S3. Calculated principal *g* values g_i and the *g* shift from a free electron Δg_i ($i = x, y, z$).

	g_x	g_y	g_z	$\boldsymbol{g}_{\mathbf{ave}}$ [a]	Δg_x	Δg_y	Δg_z
6T-H_2	2.00295	2.00092	2.00210	**2.00199**	0.00063	−0.00140	−0.00022
6T-HBr	2.00483	2.00325	2.00178	**2.00329**	0.00251	0.00093	−0.00054
6T-Br_2	2.00514	2.00722	2.00146	**2.00461**	0.00282	0.00490	−0.00086
P3HT [b]	2.00310	2.00152	2.00203	**2.00222**	0.00078	−0.00080	−0.00029

[a] The g_{ave} values are calculated by Equation S1. [b] These values were obtained from ESR measurements.[S4]

Table S3 summarizes the principal values of the calculated *g* tensors g_i and the *g* shift Δg_i ($i = x, y, z$) from a free electron (g_e = 2.002319). An average of the principal values g_{ave} was calculated as

$$g_{\mathrm{ave}} = \sqrt{g_{\mathrm{x}}^2\langle l^2\rangle + g_{\mathrm{y}}^2\langle m^2\rangle + g_{\mathrm{z}}^2\langle n^2\rangle}$$
$$l = \sin\theta\cos\phi \qquad (S1)$$
$$m = \sin\theta\sin\phi$$
$$n = \cos\theta$$

where < > represents spatial average. Here random orientation of molecules was assumed to calculate the g_{ave}. For 6T-H_2, the calculated g values agree well with the experimentaly measured ones as shown in the bottom row of Table S3. On the other hand, the g values increased by attaching bromine atom at the chain end. The g value of 6T-HBr was in good agreement with that of the broad signal observed in the LESR measurements. **Table S4** summarizes the calculated hfc constants on each atom where hfc constants of only bromines and neighbor atoms are shown to save space. The labels are shown in **Figure S10**. The hfc constants also increased by attaching bromine atom at the chain end. The increase in hfc would result in increase in peak-to-peak ESR linewidth ΔH_{pp},[S5] which is also in good agreement with the ESR signal we observed. We therefore attribute the broad signal to bromine-related polarons.

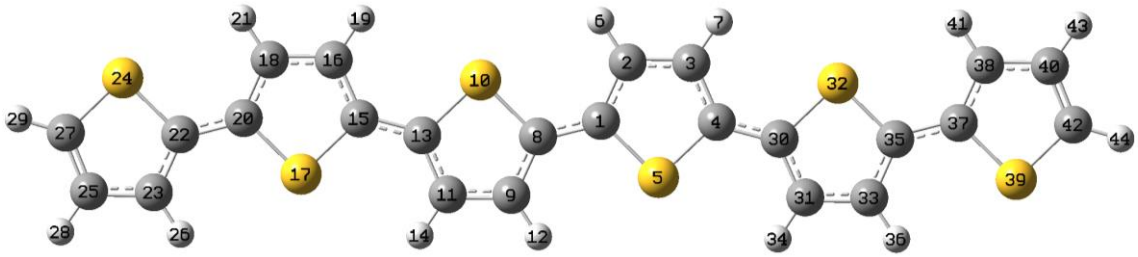

Figure S10. Atomic numbering of 6T-H_2. For 6T-HBr, no. 44 was replaced to Br. For 6T-Br_2, nos. 29 and 44 were replaced to Br.

Table S4. The hfc constants (mT) for bromines and neighbour atoms.

Label	Atom	6T-H_2	6T-HBr	6T-Br_2
		−0.02900	−0.02878	−0.02078
24	S	−0.00800	−0.00798	0.00282
		0.05970	0.05903	0.01862
		−0.21369	−0.21203	−0.19226
25	C	−0.12549	−0.12503	−0.12596
		−0.11439	−0.11393	−0.11476
		0.11571	0.11560	0.16989
27	C	0.12461	0.12440	0.18009
		0.77201	0.77190	0.87139
		−0.32712	−0.32711	−0.52893
29	X	−0.22072	−0.22081	−0.29753
		−0.08072	−0.08071	1.13027
		−0.02900	−0.02098	−0.02078
39	S	−0.00800	0.00273	0.00282
		0.05970	0.01953	0.01862
		−0.21369	−0.19451	−0.19226
40	C	−0.12549	−0.12661	−0.12606
		−0.11439	−0.11531	−0.11476
		0.11571	0.17021	0.16989
42	C	0.12461	0.18041	0.18009
		0.77201	0.87191	0.87139
		−0.32712	−0.52640	−0.52893
44	Y	−0.22072	−0.29470	−0.29753
		−0.08072	1.12410	1.13027

X = H for 6T-H_2 and 6T-HBr, Br for 6T-Br_2. Y = H for 6T-H_2, Br for 6T-HBr and 6T-Br_2.

References

[S1] D. Credgington, J. Durrant, *J. Phys. Chem. Lett.* **2012**, *3*, 1465.

[S2] T. Nagamori, K. Marumoto, *Adv. Mater.* **2013**, *25*, 2362.

[S3] M. J. Frisch, G. W. Trucks, H. B. Schlegel, G. E. Scuseria, M. A. Robb, J. R. Cheeseman, G. Scalmani, V. Barone, B. Mennucci, G. A. Petersson, H. Nakatsuji, M. Caricato, X. Li, H. P. Hratchian, A. F. Izmaylov, J. Bloino, G. Zheng, J. L. Sonnenberg, M. Hada, M. Ehara, K. Toyota, R. Fukuda, J. Hasegawa, M. Ishida, T. Nakajima, Y. Honda, O. Kitao, H. Nakai, T. Vreven, J. A. Montgomery, Jr., J. E. Peralta, F. Ogliaro, M. Bearpark, J. J. Heyd, E. Brothers, K. N. Kudin, V. N. Staroverov, R. Kobayashi, J. Normand, K. Raghavachari, A. Rendell, J. C. Burant, S. S. Iyengar, J. Tomasi, M. Cossi, N. Rega, J. M. Millam, M. Klene, J. E. Knox, J. B. Cross, V. Bakken, C. Adamo, J. Jaramillo, R. Gomperts, R. E. Stratmann, O. Yazyev, A. J. Austin, R. Cammi, C. Pomelli, J. W. Ochterski, R. L. Martin, K. Morokuma, V. G. Zakrzewski, G. A. Voth, P. Salvador, J. J. Dannenberg, S. Dapprich, A. D. Daniels, Ö. Farkas, J. B. Foresman, J. V. Ortiz, J. Cioslowski, and D. J. Fox, Gaussian 09, Revision D.01, Gaussian, Inc., Wallingford CT, 2009.

[S4] S. Watanabe, H. Tanaka, S. Kuroda, A. Toda, S. Nagano, T. Seki, A. Kimoto, J. Abe, *Appl. Phys. Lett.* **2010**, *96*, 173302.

[S5] D. Son, K. Marumoto, T. Kizuka, Y. Shimoi, *Synth. Met.* **2012**, *162*, 2451.